Effect of Debonding of Rebars on the Seismic Response of Boundary Elements of Lightly Reinforced Shear Walls

A.H. Sharifzadeh[1] and S. Tariverdilo[1*]

1. Department of Civil Engineering, Faculty of Engineering, Urmia University, Urmia, Iran

Corresponding author: s.tariverdilo@urmia.ac.ir

ARTICLE INFO

ABSTRACT

Rebar fracture in boundary elements of lightly reinforced shear walls in recent earthquakes motivated research on the minimum longitudinal reinforcement of shear walls. These researches lead to change in the ACI 318-19 requirement for minimum longitudinal reinforcement of boundary elements. New ACI 318 requirement increases minimum longitudinal reinforcement ratio for boundary elements of shear walls with low demand, that could have economic burden. This study experimentally investigates is it possible to avoid this increase in minimum rebar by debonding rebars in critical region of boundary elements in lightly reinforced shear walls. Tests includes specimens with bonded and debonded rebars, which are tested under monotonic and cyclic loading. Load protocol to account for failure types of low reinforcement shear walls is asymmetric. Test results show that out of plane buckling of specimens with debonded rebars initiates at lower axial strains that could be attributed to reduction in element lateral stiffness due to use of debonding. On the other hand debonding resulted in reduction of local strain demand on rebar. It could be concluded that larger minimum dimension for boundary elements will be required when debonding is employed.

1. Introduction

Shear walls, due to their large stiffness and energy absorbing capacity, are considered as accountable elements for seismic resistant design. Force transfer between concrete and rebars through bond stress (tension-stiffening), although increases the stiffness of reinforced concrete elements, it could be accompanied with substantial decrease in strain capacity of rebar [1]. This is mainly due to strain localization in rebars at the location of cracks. Decreasing the ratio of longitudinal reinforcement increases the crack spacing together with more localized

strain profile for rebar leading to more reduction in strain capacity of the rebar [2-3].

On the other hand, while minimum rebars in beams and columns are derived employing the concept of spreading plasticity along member length by providing ratio of 2 to 3 between flexural strength and cracking strength [4], this is not the case for shear walls. For shear walls similar to slabs, the main concept in calculating minimum reinforcement is crack spacing and width in concrete [2]. This resulted in very different ratio of longitudinal rebars for beams and columns versus shear walls, while this ratio is about 0.004 for beams and columns, it is about 0.0025 for walls [5]. As discussed in preceding paragraph, smaller ratio of longitudinal rebars results in more localized strain profile for rebar and could lead to rebar fracture. This is exactly what was happened in 1985 Chile earthquake where longitudinal rebars of lightly reinforced bearing walls in eight story building was fractured. The same type of collapse is again found in 2010/2011 Canterbury earthquakes, leading to collapse of several multi story buildings [6].

These failures show that while main emphasis in boundary elements of shear walls is on its compression response [7,8], its response under mainly tensile loading could be crucial. Accounting for these observed failures, there are increased attention at failure modes of lightly reinforced walls [9-12]. These efforts concluded in increased longitudinal reinforcement ration for boundary elements of shear walls in amendment 3 of NZS 3101-06 [13] and later in ACI 318-19 [5].

Increasing the minimum ratio of longitudinal reinforcement is not the only way to reduce the risk of rebar fracture at possible plastic hinge location. It is well known that debonding of reinforcement could be employed to avoid localization of strain in rebars and even it is a recommended practice in ACI 318-19 to provide adequate stretching length for anchor bolts. Shimazaki experimentally investigated the effect of debonding on the repairability of coupling beams with diagonal reinforcement [14]. He showed that debonding by inducing uniform distribution of strain in diagonal rebars, reduces repair cost and increases energy absorption capacity of the element. Patel et al. 2015 investigated the effect of rebars rib spacing and height on its strain profile under monotonic tensile loading [15]. They found that decreasing rib height (which in fact means debonding it from surrounding concrete) reduces the number of cracks, increases crack width and strain penetration depth and yield penetration.

Under cyclic loading, concentrated cracks in boundary element reduces its lateral stiffness. Even at small axial displacements, this reduction in lateral stiffness leads to out of plane buckling (OOPB). Paulay and Preistley [16] assessing results of experimental works on boundary elements, developed a correlation between average axial deformation and beginning of OOPB. Rosso et al. [17] investigated boundary elements of thin lightly reinforced walls that are commonly used in south America. They found that cracking pattern largely affects the tensile strain initiating OOPB. Kowalsky et al. [18] developed a comprehensive experimental program on boundary elements of ductile shear walls using different loading protocols. They found that increasing the ratio of longitudinal reinforcement increases susceptibility to OOPB.

This paper investigates effect of rebar debonding on the strain localization of longitudinal reinforcements in lightly reinforced boundary elements of shear walls. Sample tests are designed to replicate boundary elements of lightly reinforced shear walls. Monotonic and cyclic tests are carried out to investigate the effect of debonding on cracking pattern, reinforcement strain profile and out of plane instability in boundary elements.

2. Evaluating Strain Profile and out of Plane Buckling

Strain penetration (SP) into foundation and on either side of cracks, tension stiffening (TS) and localization of rebar fracture (RF) complicates derivation of actual strain profile of rebar from test results. In the same time, beginning of OOPB is related to mean rebar axial strain. Evaluation of this average strain at least requires eliminating the effect of strain penetration (ST). Therefore, it seems necessary to develop a procedure to obtain actual uniform strain of the rebar. This section develops this procedure and describe various strain measures and correlation between rebar strain and OOPB that should be verified for testes specimens.

Altheeb et al. [19] and Patel et al. designed tests to evaluate strain penetration in boundary elements of shear walls. Tests by Patel et al. for rebars with standard rib conforming to NZS 3101-6 with yield stress of 300 MPa gave a strain penetration length about $3.6d_b$ on either side of crack (l_{sp}). However as could be expected, tests by Altheeb shows that strain penetration length is not fixed and depends on the rebar strain. Based on the finding of Altheeb et al., Figure 1 shows how this length changes with rebar strain. As could be seen extent of variation in

strain penetration length is quite significant. In the treatment of experimental results this depends should be accounted for.
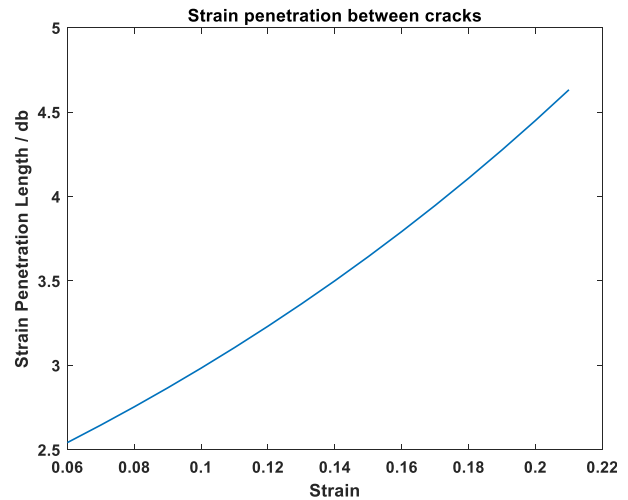

Fig. 1. Evolution of strain penetration length between cracks with rebar strain based on experimental results of Altheeb et al. [19].

Slip due to strain penetration in foundation could be calculated using simple bond-slip models, such as that developed by Sezen and Setzler [20]. Assuming uniform bond stress and its reduction from $\sqrt{f_c'}$ for rebar strains (ε_s) smaller that yield strain (ε_y), to $\alpha\sqrt{f_c'}$ for strains larger than ε_y, slip due to strain penetration into foundation (Δ_{slip}) could be evaluated in closed form as

$$\Delta_{slip} = \frac{\varepsilon_s f_s d_b}{8\sqrt{f_c'}} \qquad\qquad \varepsilon_s \leq \varepsilon_y \qquad (1)$$

$$\Delta_{slip} = \frac{\varepsilon_s f_s d_b}{8\sqrt{f_c'}} + \frac{(\varepsilon_s + \varepsilon_y)(f_s - f_y)d_b}{8\alpha\sqrt{f_c'}} \quad \varepsilon_s \geq \varepsilon_y$$

where f_s, f_y, d_b are rebar actual stress, yield stress and diameter; f_c' is concrete compressive strength; and α is assumed to be 0.5 by Sezen and Setzler. Constant α does not accounts for reduction in bond stress with increasing strain in rebar. To account for decrease in bond stress in larger strains, in

this study, it is assumed that α evolves with rebar strain as follows

$$\alpha = 0.81 - 1.43\varepsilon_s \geq 0.5 \qquad (2)$$

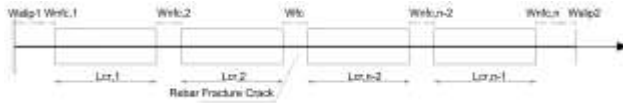At the final stage of the test, assumed strain field in the specimen is depicted in Figure 2.

Fig. 2. Notations used in analysis of strain field.

Tension stiffening, due to force transfer from rebar to surrounding concrete between cracks, reduces rebar stress in uncracked segments and consequently reduces total deformation. At final stages of test, strain in total length is well above yield strain, therefore use of bond stress of $\alpha\sqrt{f_c'}$ could be a valid assumption. With these assumptions, stress in the rebar midway between cracks for segment i will be

$$\Delta f_{s,i} = \alpha\sqrt{f_c'}\,\pi d_b \frac{L_{cr,i}}{2} \qquad (3)$$

$$\Delta\varepsilon_{s,i} = \frac{\Delta f_{s,i}}{E_{sh}}$$

where i denotes element segment i between cracks (see Figure 2); $L_{cr,i}$, $\Delta f_{s,i}$, $\Delta\varepsilon_{s,i}$ are length and decrease in rebar stress and strain at midway between cracks all in segment i and E_{sh} is rebar strain hardening ratio.

Now integrating rebar strain between cracks, it will be straight forward to calculate rebar deformation between cracks. The total deformation minus slip due to strain penetration into foundation will be

$$\Delta_{total} - W_{slip} = \Delta_{ts} + \Delta_{nfc} + \Delta_{fc} = \qquad (4)$$

$$\sum_{i=1}^{N_{cracks}-1}\left(\int_0^{L_{cr,i}} \varepsilon_s\,dx + W_{nfc,i}\varepsilon_{nfc,i}\right) + (W_{fc} + l_{sp})\varepsilon_{fc}$$

here Δ_{ts}, Δ_{nfc} and Δ_{fc} are deformation components due to rebar elongation between cracks, at cracks where no rebar fracture occurs and at crack with rebar fracture, respectively.

Rebar stress in strain hardening range could be evaluated from relation proposed by Mander et al. [21]

$$f_s = f_{su} + (f_y - f_{su})\left(\frac{\varepsilon_{su} - \varepsilon_s}{\varepsilon_{su} - \varepsilon_{sh}}\right)^P \qquad (5)$$

$$P = E_{sh}\frac{\varepsilon_{su} - \varepsilon_{sh}}{f_{su} - f_y}$$

Knowing the maximum force in the test and using equation 5, it is possible to evaluate ε_{nfc}, then using cracking pattern, two deformation terms Δ_{ts} and Δ_{nfc} could be calculated. Now the third term of deformation (Δ_{fc}) and then ε_{fc} could be computed. Considering the total length of fractured crack ($W_{fc} + l_{sp}$), ε_{fc} should be on the same order of elongation interpolated from test results in Table 1 accounting for *actual length of fracture i.e. $W_{fc} + l_{sp}$*.

Different estimates of average strain of the rebar are evaluated in three ways

1) Ignoring strain penetration and dividing total elongation (Δ_{total}) by elements length (l) giving ε_{sm1}.
2) Reducing elongation due to strain penetration into foundation (Δ_{slip}) from total elongation and dividing calculated elongation ($\Delta_{total} - \Delta_{slip}$) by the element length (l) giving ε_{sm2}.
3) Based on the presented analytical treatment and computing ε_{nfc}, which is a better estimate of actual uniform elongation.

Extensive tensile cracking of boundary elements could lead to instability in the form

out of plane buckling (OOPB) of whole specimen. Accounting for single layer of reinforcements, OOPB beginning load depends on average tensile strain experienced by the rebar (ε_{sm}) between cracks and the element length (l) and dimension (b) by the following relation [3]

$$\frac{l}{b} = \frac{1}{0.5\sqrt{\varepsilon_{sm} - 0.005}} \tag{6}$$

3. Experimental Program

Tests are conducted using universal jack of 1000 kN capacity universal jack of center for infrastructure research at Urmia University. Small moment gradient along shear wall height results in nearly uniform uniaxial loading on its boundary elements. This small moment gradient results in nearly constant axial loading on boundary elements of shear walls. Consequently it is common to test boundary elements of shear walls using specimens under uniaxial loading ([8-9, 18-19]).

To study the effect of debonding on deformation capacity of boundary elements of lightly reinforced shear walls, monotonic and cyclic tests on bonded and debonded samples are designed. Table 1 gives description of samples considered in this study. Samples reinforcements and dimensions are depicted in Figure 3. Three linear variable differential transformer (LVDT) are used to measure axial displacement and gauges are employed to monitor cracks opening and lateral deflection.

Table 1. Samples description, geometry and reinforcement.

| Sample Designation	Descrption	Debonding Length (mm)
BM2	**Bonded** sample 2 under **Monotonic** loading	-
BM3	**Bonded** sample 3 under **Monotonic** loading	-
BC1	**Bonded** sample 1 under **Cyclic** loading	-
BC2	**Bonded** sample 2 under **Cyclic** loading	-
DC1	**Debonded** sample 1 under **Cyclic** loading	80
DC3	**Debonded** sample 3 under **Cyclic** loading	220
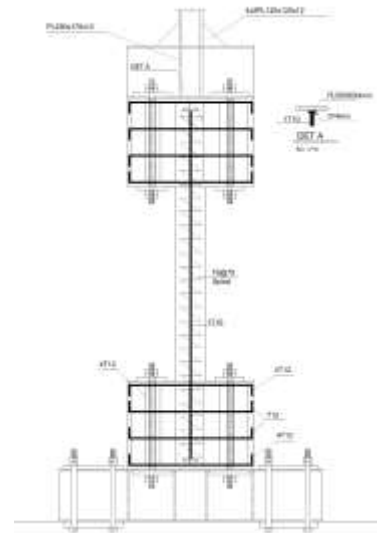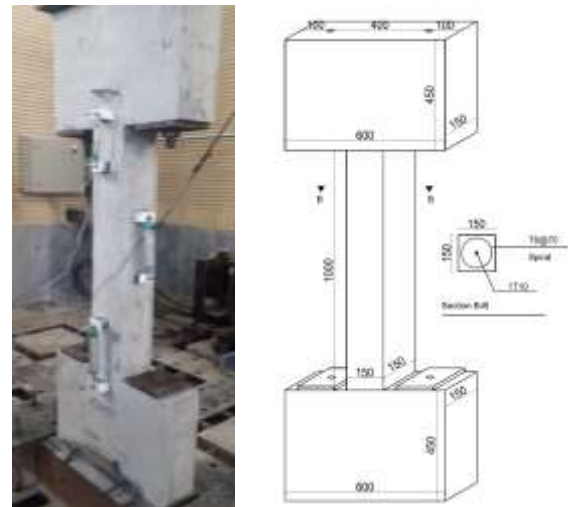
Fig. 3. Specimens shape and loading.

In lightly reinforced shear walls under cyclic loading, concrete does not undergo large compression loading and failure demonstrates itself in the form of tensile cracking and compression buckling rather than compression failure (spalling). Accounting for this and following Hilson et al. [23] and Rosso et al. [17], an asymmetric loading protocol is adopted for cyclic loading mainly introducing tensile loading on the sample with small compression strain on the order 0.003.

Table 2. Material properties for concrete and reinforcements.

Designation	Material Property	Reinforcements
f_y	Yield Stress (MPa)	433
f_{su}	Ultimate Strength (MPa)	622
ε_{fc_test}	Fracture Elongation in $5d_b$	0.30
	Fracture Elongation in $10d_b$	0.27
	Fracture Elongation in 200 mm	0.21
	Material Property	**Concrete**
f_c'	28 days strength (MPa)	30

Loading protocol is symmetric until reaching compression strain of 0.003, then protocol becomes asymmetric, where maximum compression strain remains constant and meanwhile tensile strain increases in the following load steps. Figure 4 depicts loading protocol used in this study. Table 2 gives materials properties used in the experiments.

(a)

(b)
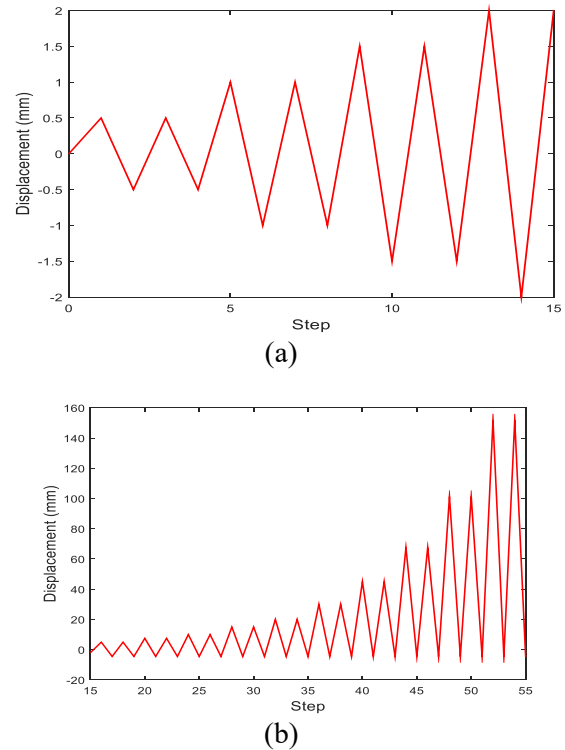
Fig. 4. Loading protocol used in the experiments, a) symmetric loading in small displacements, b) asymmetric loading in large displacements.

4. Bonded specimens under monotonic loading

Three specimens are designed to study strain profile of bonded longitudinal rebars under monotonic loading, but during transfer of specimens, specimen BM1 extensively cracked and although it was tested, its results will not be apealing. Therefore in the following only results for BM2 and BM3 are reported. Figure 5a shows load-deflection result and Figure 5b gives the cracking pattern of the specimens. As could be seen, the cracking pattern are nearly the same but the cracking sequence, width and maximum axial force are different (Table 3). In the both cases, rebar fracture has occurred in the crack at element-foundation interface.
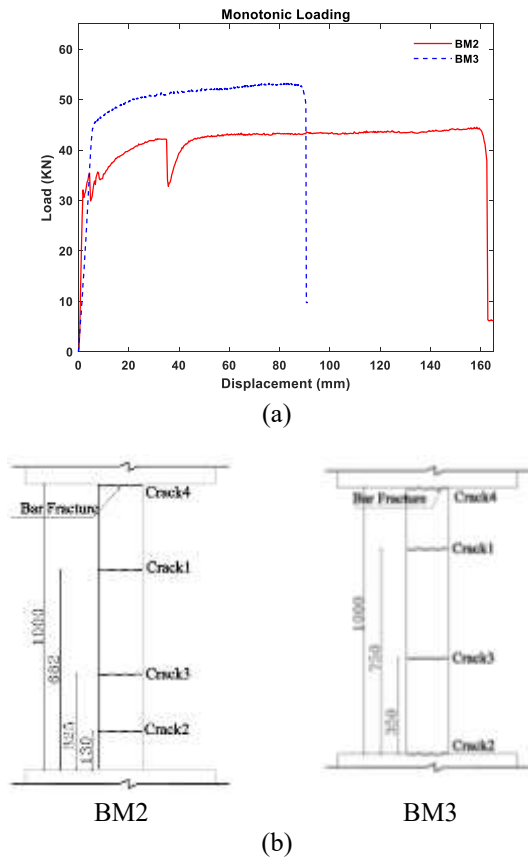
(a)

BM2   BM3

(b)

Fig. 5. Test results for bonded specimens under monotonic loading, a) load-deflection, b) cracking pattern.

Table 3 gives different estimates of strain in the rebar. As could be seen, estimates of the average strain from different methods defined in section 2 are different. This table shows that accounting for strain penetration into foundation does not improve estimate of average strain estimation, i.e. ε_{sm2} is not a better estimator of average strain than ε_{sm1}. In fact, estimate of elongation based on gross deformation (ε_{sm1}), although is slightly larger than actual uniform strain ε_{nfc}, gives better estimate of actual deformation compared to ε_{sm2}, which is important in evaluation of element susceptibility to OOPB. This is mainly due to large ratio of the specimen length to the rebar fracture elongation (Δ_{fc} in Equation 4). Therefore fracture of

reinforcement have little impact on the axial deformation observed in the tests and average strain ε_{sm1} gives a conservative estimate of uniform elongation ε_{nfc}. Accounting for this, average strain in the specimens under cyclic loading are evaluated using ε_{sm1}.

Table 3. Evaluation of different strain estimates for bonded samples under monotonic loading.

Sample Desig.	Crack Number and Width (mm)				Total Elong.	Average Strain ε_{sm1}	Average Strain ε_{sm2}
	1	2	3	4			
BM2	20	17	35	91[*]	163	0.163	0.119
BM3	31	11	29	20[*]	91	0.091	0.068
[*] Rebar fracture crack							

Sample Desig.	See Fig. 2		Elongation			$\varepsilon_{sm1}/\varepsilon_{nfc}$	$\varepsilon_{sm2}/\varepsilon_{nfc}$
	W_{slip}	l_{sp}	ε_{nfc}	ε_{fc}	ε_{fc_test}		
BM2	25.8	36	0.14	0.22	0.27	1.12	0.79
BM3	12.2	27	0.08	0.29	0.32	1.14	0.85

Table 3 also shows that same specimens with relatively same cracking pattern could give different axial deformation at failure and even estimate of uniform strain (ε_{nfc}) could be quite different.

5. Bonded specimens under cyclic loading

Figure 6 gives test results for bonded samples tested under cyclic loading, where load step initiating out of plane buckling is marked on the figure. The figure also shows cracking pattern and photo of the specimens at the end of tests. Cracking pattern for the specimens shows that pattern is quit similar to that observed for monotonic loading with the exception of additional cracks for BC1, which are developed mainly after buckling of specimen. While in specimens under monotonic loading due to strain penetration

into foundation, rebar fracture for the both specimens BM2 and BM3 is occurred at foundation-element interface, this is not the case for specimens under cyclic loading. The reason for this change in fracture location is out of plane buckling (OOPB). OOPB results in concentration of strain demand in mid-span region and consequently all of the rebar fracture for these specimens are occurred at mid-span region.

After specimen buckling, cracks width are not representative of pre-buckling strain profile. Therefore no analysis to drive uniform elongation is done on these specimens. Table 4 gives cracks width and order at which cracks taking place. Although the number and pattern of cracking is different for the specimens, OOPB occurred at same average strain for the both specimens, which confirms correlation between OOPB and average axial deformation.
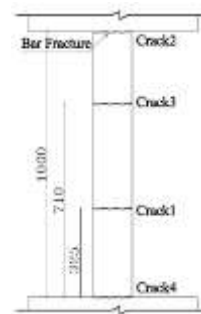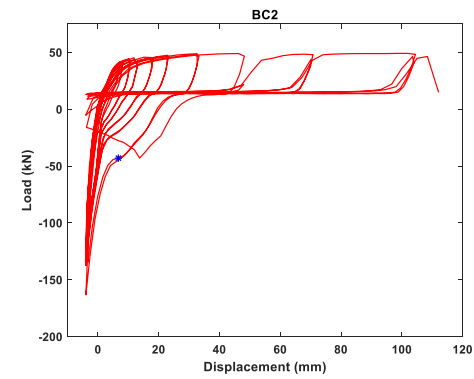
Table 4. Evaluation of strain estimates for bonded samples under cyclic loading at OOPB and test end.

Sam.	Status	Crack Number and Width (mm)						Total Elong.	ε_{sm1}	ε_{sm2}
		1	2	3	4	5	6			
BC1	OOPB	5	4	9	7	7	-	32	0.033	0.032
	Test End	20	19	14*	21	25	12	111	0.111	-
BC2	OOPB	10	5	9	8	-	-	32	0.032	0.031
	Test End	25	19*	22	18	-	-	84	0.084	-

* Rebar fracture crack
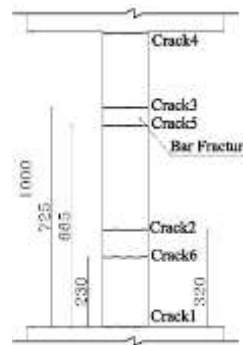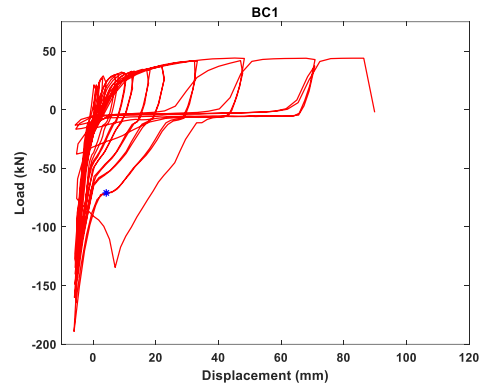
(a)

(b)

Fig. 6. Load-displacement and cracking pattern for specimens, a) BC1, b) BC2.
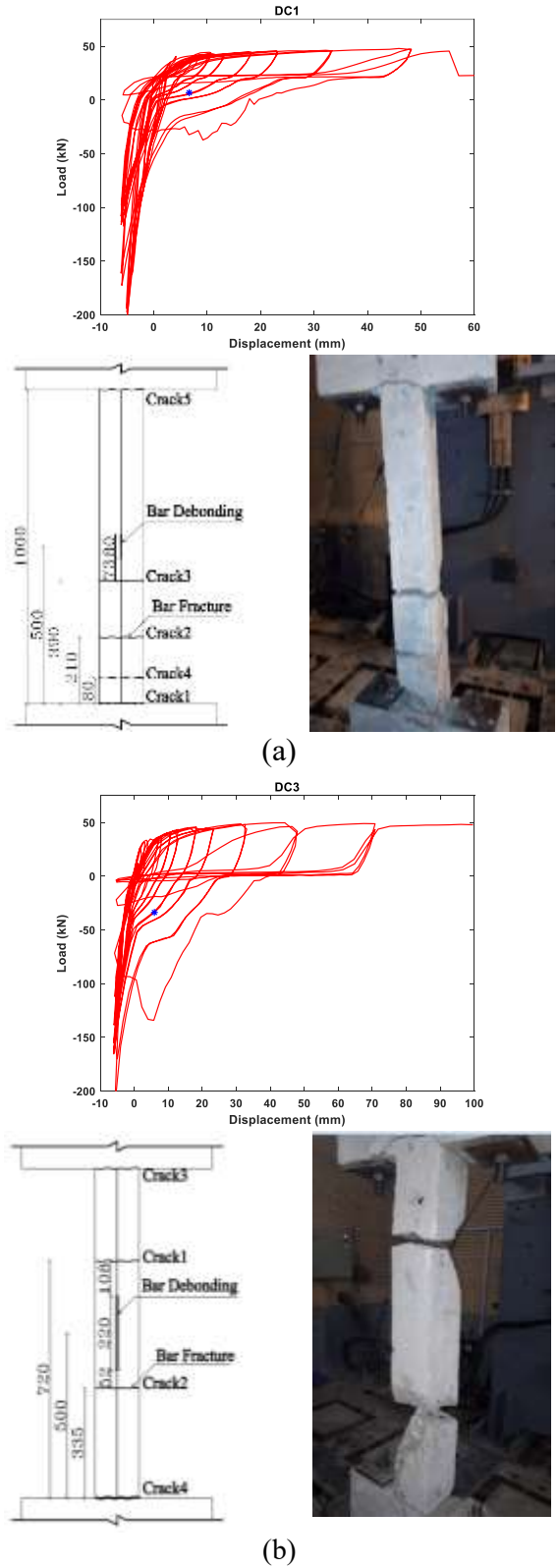
6. Debonded Specimens under Cyclic Loading

Two debonded specimens are tested under cyclic loading. Debonding is done using polyurethane sleeves around rebars. Figure 7 gives the load-displacement of the debonded samples with different debonding length of 80 and 220 mm, where debonding length located at the samples midpoint. OOPB beginning point is also depicted on the load-displacement graph. Cracking pattern and samples photo at the end of test are also given in Figure 7.

Table 5. Evaluation of strain estimates for debonded samples under cyclic loading at OOPB and test end.

Sam.	Status	Crack Number and Width (mm)					Total Elong.	ε_{sm1}
		1	2	3	4	5		
DC1	OOPB	3	6	5	4	-	18	0.018
	Test End	7	24*	23	6	5	65	0.065
DC3	OOPB	5	7	2	4	-	18	0.022
	Test End	24	36*	6	32	-	98	0.098
* Rebar fracture crack								

Test results show that debonding rebars has resulted in development of cracks at a distance about $5d_b$ to $7.5d_b$ from the end of debonding length and cracks adjacent to the debonding length has largest width. This is anticipated as this crack releases deformation allocated in the deboned length. Table 5 gives crack number in order of occurrence and its width at beginning of OOPB and at test end. As could be seen, in the both samples OOPB occurs at same axial deformation, which is smaller than that for bonded samples. This is an indication of smaller lateral stiffness of specimen, which is expected due to elimination of tension stiffening in debonding length.

(a)

(b)

Fig. 7. Debonded specimens under cyclic loading, load-displacement, cracking pattern and photo at the end of tests.

This smaller lateral stiffness resulted in larger lateral deflection, larger rebar strain in cracks and therefore smaller number of cycles are require for fracture of the rebar due to low cycle fatigue. The crack adjacent to the debonding length has largest crack width and in the both cases fracture occurs at these cracks. The main contributing factor for this pattern of failure is that these cracks are near the mid span, where the element has largest curvature, and it seems that debonding is not detrimental in this respect.

Increase in debonding length resulted in an increase in crack width for the crack near debonding length. However it does not affect the OOPB initiating axial strain and also the maximum axial deformation that the specimen experiences.

7. Rebar Strain Initiating out of Plane Buckling

Correlation between rebar strain triggering specimen buckling and slenderness ratio for bonded and debonded samples is depicted in Figure 8, which shows that debonded specimens buckles at smaller axial displacements. As discussed in the previous section, this is mainly due to debonding of rebars that leads to reduction in specimen lateral stiffness. This figure also shows prediction of Equation 6 for axial strain triggering OOPB that is unconservative for both of the bonded and debonded specimens.

ACI 318-19 requires a minimum boundary element dimension of at least $h_u/16$, where h_u (l in this paper) is laterally unsupported height of boundary element. Using Equation (6) it is possible to back calculate target minimum tensile strain of BE as

$$\frac{h_u}{b_{min}} = 16 = \frac{1}{0.5\sqrt{\varepsilon_{sm} - 0.005}} \rightarrow \varepsilon_{sm} = 0.021 \qquad (7)$$

In other word, ACI limitation of minimum dimension for BE guarantees reaching a minimum tensile strain of 0.021. Referring to Table 3 and 4 axial tensile strain at the beginning of OOPB for bonded and debonded specimens are about 0.032 and 0.020, respectively. Noting that l/b of the specimens is about 9.3, the specimens (bonded/deboned) should reach a tensile strain of about 0.057 (see Figure 8). It could be concluded that both of the bonded and debonded specimens fail to reach a minimum target tensile strain of ACI, while their l/b is about 9.3, well below ACI minimum l/b of 16.
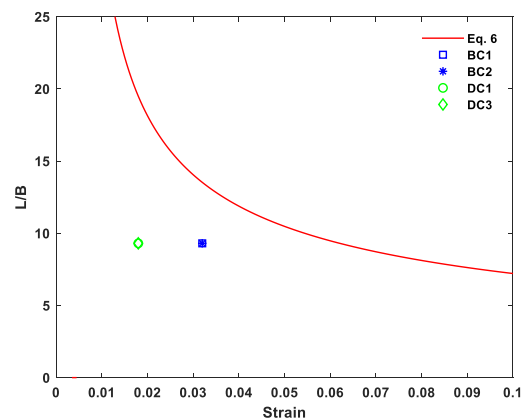

Fig. 8. Correlation between rebar tensile strain and out of plane buckling.

Conclusion

Performance of rebar debonding in boundary elements of lightly reinforced shear walls investigated experimentally. Tests are developed to evaluate effect of debonding on strain profile and out of plane buckling of boundary elements. Experiment include monotonic tests on bonded specimens and cyclic tests on bonded and debonded

specimens. Test results leads to the following conclusions

- Debonding provides additional source of deformation in the vicinity of terminating points of debonding and does not affects axial deformation capacity of the specimens.
- Debonding by reducing lateral stiffness of the specimen leads to out of plane buckling in smaller axial strains compared to the bonded specimens, which means larger minimum dimension will be required for boundary elements with debonded rebars.
- ACI 318-19 requires a minimum boundary element dimension (b_{min}) of at least $l/16$, where l is laterally unsupported height of the boundary element. This limitation intends to provide a minimum tensile strain capacity of 0.021 for BEs with l/b of 16.
- While l/b of specimens is about 9.3 maximum available tensile strain before out of plane buckling for bonded and debonded specimens are about 0.020 and 0.032, well below anticipated tensile strain capacity of the elements.
- Comparing maximum tensile strain of specimens at beginning of OOPB, elements with debond rebars seem more vulnerable to OOPB. This means that minimum dimension of the element for debonded rebars should be larger than that for elements with bonded rebars. Further researches are required to quantify this increase.
- Uniform axial strain in the specimens up to rebar fracture could be approximated by total axial deformation, ignoring strain penetration and tension stiffening.

REFERENCES

Eligehausen, R., Ozbolt, J., Mayer, U. (1998). "Contribution of concrete between cracks at inelastic steel strains and conclusion for the optimization of bond, Bond and development of reinforcement." SP 180, American Concrete Institute, Farmington Hills, MI, pp. 45-80.

Collins, M.P., Mitchell, D. (1990). "Prestressed Concrete Structures." Prentice-Hall Inc., Englewood Cliffs, NJ, 766 p.

Mohle, J. (2015). "Seismic Design of Reinforced Concrete Buildings." McGraw-Hill, 760 p.

CEB-FIP. (2007). "Bulletin 39: Seismic Bridge Design and Retrofit – Structural Solutions, International Federation for Structural Concrete", Lausanne, Swiss.

ACI 318-19. (2019). "Building code requirements for structural concrete (ACI 318-19) and commentary." American Concrete Institute, Farmington Hills, MI.

Lu, Y., Henri, R.S., Ma, Q.T. (2014). "Numerical modelling and testing of concrete walls with minimum vertical reinforcement." NZSEE conference.

Arteta, C.A., To, D.V., Moehle, J.P. (2014). "Experimental response of boundary elements of code-compliant reinforced concrete shear walls." Tenth U.S. National Conference on Earthquake Engineering: Frontiers of Earthquake Engineering, Anchorage, Alaska.

Cook, D.T., To, D., Moehle, J. (2012). "Ductility of RC shear wall boundary element in compression." PEER Internship Program.

Sritharan, S., Beyer, K., Henry, R.S., Chai, Y.H., Kowalsky, M., Bullf, D. (2014). "Understanding Poor Seismic Performance of Concrete Walls and Design Implications." Earthquake Spectra, Vol. 30, Issue 1, pp. 307-334, doi:10.1193/021713EQS036M.

Hoult, R.D., Goldsworthy, H.M., Lumantana, E. (2016). "Displacement capacity of lightly reinforced rectangular concrete walls." Australian Earthquake Engineering Society 2016 Conference, Melbourne, Victoria.

Hoult, R.D., Goldsworthy, H.M., Lumantana, E. (2016). "Seismic Performance of lightly reinforced and unconfined C-saped walls." Australian Earthquake Engineering Society 2017 Conference, Canberra, ACT.

Lu, Y., Henry, R.S., Gultom, R., Ma, Q.T. (2017). "Cyclic testing of reinforced concrete walls with distributed minimum vertical reinforcement." ASCE Journal of Structural Engineering, Vol. 143, Issue 5, doi:10.1061/(ASCE)ST.1943-541X.0001723.

NZS 3101 (2006). "Concrete structures standard (Amendment 3)." Wellington, New Zealand.

Shimazaki, K. (2004). "De-Bonded Diagonally Reinforced Beam for Good Repairability." 13th World Conference on Earthquake Engineering, Vancouver, B.C., Canada, Paper No. 3173.

Patel, V.J., , Van, B.C., Henry, R.S., Clifton, G.C. (2015). "Effect of reinforcing steel bond on the cracking behaviour of lightly reinforced concrete members." Construction and Building Materials, Vol. 96, Issue 2, pp. 238–247, doi.org/10.1016/j.conbuildmat.2015.08.014 .

Paulay, T., and Priestley, M. J. N., (1993). "Stability of ductile structural walls." ACI Structural Journal, Vol. 90, Issue 4, pp. 385–392.

Rosso, A., Jimenez-Roa, L.A., Almeida, J.P., Blando, C.A., Bonett, R.L., Beyer, K. (2018). "Cyclic tensile-compressive tests on thin concrete boundary elements with a single layer of reinforcement prone to out-of-plane instability." Bulletin of Earthquake Engineering, Vol. 16, Issue 2, pp. 859-887, doi:10.1007/s10518-017-0228-1.

Haro, A.G., Kowalsky, M., Chai, Y.H., Luciera, G.W. (2018). "Boundary Elements of Special Reinforced Concrete Walls Tested under Different Loading Paths." Earthquake Spectra, Vol. 34, Issue 3, pp. 1267-1288, doi:10.1193/081617EQS160M.

Altheeb, A., Albidah, A., Lam, N.T.K., Wilson, J. (2013). "The development of strain penetration in lightly reinforced concrete shear walls.", Australian Earthquake Engineering Society 2013, Hobart, Tasmania.

Sezen, H., Setzler, E.J. (2008). "Reinforcement slip in reinforced concrete column." ACI Structural Journal, Vol. 105, Issue 3, 280-288.

Mander, J.B., Priestley, M.J.N., Park, R. (1984). "Seismic design of bridge piers." Report 84-02, Department of Civil Engineering, University of Canterbury, Christchurch, New Zealand.

Hilson, C.W., Segura, C.L., Wallace, J.W. (2014). "Experimental study of longitudinal reinforcement buckling in reinforced concrete structural wall boundary element." Tenth U.S. National Conference on Earthquake Engineering: Frontiers of Earthquake Engineering, Anchorage Alaska.